

# Optical Properties of 2D Semiconductor WS<sub>2</sub>

Chunxiao Cong,\* Jingzhi Shang, Yanlong Wang, and Ting Yu\*

2D semiconductor tungsten disulfide (WS<sub>2</sub>) attracts significant interest in both fundamental physics and many promising applications such as light emitters, photodetectors/sensors, valleytronics, and flexible nanoelectronics, due to its fascinating optical, electronic, and mechanical properties. Herein, basic exciton properties of monolayer WS<sub>2</sub> are reviewed including neutral excitons, charged excitons, bounded excitons, biexcitons, and the effects of electrostatic gating, chemical doping, strain, magnetic field, circular polarized light, and substrate on these excitonic structures. Besides basic excitonic emission, single-photon emission, exciton–polaritons, and stimulated emission in monolayer WS<sub>2</sub> are also discussed. The understanding of these optical phenomena is critical for the development of potential optical applications in electronic and optoelectronic devices. Finally, a summary and future perspective of the challenges and developments regarding 2D semiconductor WS<sub>2</sub> is presented.

its unique properties such as large spin–orbit coupling ( $\approx 420$  meV), high emission quantum yield,<sup>[18]</sup> large exciton/trion binding energy,<sup>[19–21]</sup> nonblinking photon emission,<sup>[21]</sup> and so on. The most common and stable stacking structure of WS<sub>2</sub> is 2H, in which the W atoms of a given layer are sitting exactly on top of the S atoms of its neighboring layer. Bulk and multilayer WS<sub>2</sub> are indirect-gap semiconductors. Interestingly, when thinning down to 1L thickness, it converts into a direct-gap semiconductor with the energy gap of  $\approx 2$  eV.<sup>[22]</sup> Therefore, it presents strong photoluminescence (PL).<sup>[23]</sup> Combined with the relatively low defect density in WS<sub>2</sub>, 1L WS<sub>2</sub> shows a higher PL quantum yield ( $\approx 6\%$ ) than other 2D semiconductors (compared to  $\approx 0.1\%$  in 1L MoS<sub>2</sub>).<sup>[18]</sup>

## 1. Introduction

2D layered materials, such as graphene and transition metal dichalcogenides (TMDs), have aroused great interest during the last decade because of their extraordinary properties for both fundamental physics and promising potential applications.<sup>[1–16]</sup> Though graphene has very high mobility, there is a key bottleneck for graphene-based transistors that its on-off ratio is very small due to the inherent gapless band structure of graphene.<sup>[1,17]</sup> Superior to graphene, monolayer (1L) TMDs with native direct bandgaps in the visible and near-infrared range have begun to attract increasing attention as 2D semiconductors. TMDs with common formula MX<sub>2</sub> (M = Mo, W; X = S, Se), as representative prototype systems of 2D semiconductors, have been widely and intensively studied. Among them, 1L tungsten disulfide (WS<sub>2</sub>) is attracting a growing interest due to

Furthermore, due to the breaking of inversion symmetry and strong spin–orbital coupling in 1L WS<sub>2</sub>, the electronic states of the two valleys have different chiralities and lead to the valley-selective circular dichroism behavior.<sup>[24–26]</sup> This motivates significant interest in manipulating the spin and valley degrees of freedom and development of novel valleytronics. All these interesting and exceptional properties, plus the newly disclosed biexciton,<sup>[27,28]</sup> single-photon emission,<sup>[29]</sup> exciton–polaritons,<sup>[30]</sup> and stimulated emission<sup>[31]</sup> in 1L WS<sub>2</sub>, make it promising candidate for applications in next-generation nanoelectronics, optoelectronics, spintronics, and valleytronics. Herein, we review the emerging optical properties of 1L WS<sub>2</sub>. We first highlight recent progress in the basic exciton properties of 1L WS<sub>2</sub> including neutral excitons, charged excitons, bounded excitons, biexcitons, and the modulation of these basic exciton properties. Second, single-photon emission, exciton–polaritons, stimulated emission, electroluminescence, harmonic generation, dark excitons, and exciton dynamics in 1L WS<sub>2</sub> are also reviewed. In the end, we provide a summary and an outlook of the challenges and potential developments in 1L WS<sub>2</sub>.

## 2. Fundamental Excitonic Emission of 2D WS<sub>2</sub>


### 2.1. Neutral Excitons and Trions

PL spectroscopy has been shown to serve as a powerful technique to study the rich physics related to 2D WS<sub>2</sub>, such as strong Coulomb interaction,<sup>[19,27]</sup> indirect-direct bandgap transition from multilayer to 1L counterpart,<sup>[32]</sup> and giant spin-valley coupling.<sup>[25,26]</sup> The weak dielectric screening in 2D WS<sub>2</sub> leads to the enhanced Coulomb interaction, thereby making the excitons stable even at room temperature (RT) with large binding energies.<sup>[19–21,27]</sup> **Figure 1** shows the calculated band structure

Prof. C. X. Cong  
School of Information Science and Technology  
Fudan University  
Shanghai 200433, China  
E-mail: cxcong@fudan.edu.cn

Dr. J. Shang, Prof. T. Yu  
Division of Physics and Applied Physics  
School of Physical and Mathematical Sciences  
Nanyang Technological University  
Singapore 637371, Singapore  
E-mail: yuting@ntu.edu.sg

Dr. Y. L. Wang  
Key Laboratory of Chemical Lasers  
Dalian Institute of Chemical Physics  
Chinese Academy of Sciences  
Dalian 116023, China

 The ORCID identification number(s) for the author(s) of this article can be found under <https://doi.org/10.1002/adom.201700767>.

DOI: 10.1002/adom.201700767

and PL features as a function of layer thickness in  $\text{WS}_2$ .<sup>[22]</sup> As can be seen in Figure 1a, 1L  $\text{WS}_2$  has a direct bandgap with both of the conduction band minimum and valence band maximum (VBM) located at *K*-point in the Brillouin zone, so it shows a strong light emission marked by A peak corresponding to the direct excitonic transitions (Figure 1e,f). The increased layer thickness leads to the transition from direct to indirect bandgap in few-layer  $\text{WS}_2$  (Figure 1b–d), which can be proved by the lower quantum efficiency and appearance of the I peak corresponding to the indirect optical transition from PL observations (Figure 1e,f). Furthermore, strong spin–orbit coupling and interlayer coupling (only applicable to few-layer  $\text{WS}_2$ ) lead to splitting in the VBM, as shown in Figure 1a–d. This splitting results in the observation of the relatively weak B peak in addition to prominent A peak in PL spectra.<sup>[22]</sup> Though the positions of A and B exciton vary with sample thickness, the A-B splitting energy is found to be independent of layer numbers (Figure 1g),<sup>[22]</sup> which is confirmed by absorption spectra.<sup>[32]</sup> This observation is due to the strong spin-valley coupling, which fully suppresses interlayer hopping at the local valence band extrema near *K*-points as a result of the sign change of the spin-valley coupling from layer to layer in the 2H stacking order.<sup>[22]</sup>

According to the single-particle picture, after an electron is excited from the valence band (VB) to the conduction band (CB) by light with energies more than the bandgap energy, the opposite process will lead to the PL when the excited electron recombines with the hole. In 2D  $\text{WS}_2$ , the electrons and holes attract each other through strong Coulomb interaction, which makes the excitonic effects dominate the optical transitions and can be more accurately described by excitonic picture.<sup>[33]</sup> This section mainly reviews the tunable features of neutral excitons (a bounded state of an electron–hole pair) and charged excitons (a bounded state of one exciton and additional electron or hole) modulated by electrostatic gating,<sup>[19,27]</sup> molecule doping,<sup>[34]</sup> strain,<sup>[35]</sup> substrate,<sup>[36]</sup> and plasmonic and photonic enhancement<sup>[37–39]</sup> in 1L  $\text{WS}_2$ . We also introduce the circular dichroism of exciton as a powerful way to explore the valley physics related to 1L  $\text{WS}_2$ .<sup>[25]</sup>

### 2.1.1. Electrostatic Gating Effects

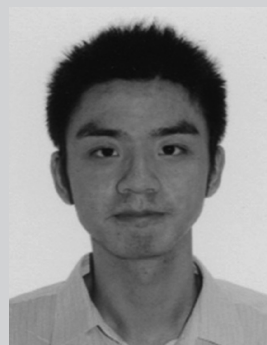
Shang et al. have reported the tunable light emissions of neutral and charged excitons in 1L  $\text{WS}_2$  by electrostatic gating.<sup>[27]</sup> Figure 2a shows the PL spectra of 1L  $\text{WS}_2$  at different back gate voltages ranged from  $-40$  to  $40$  V, which continuously modulates the density of charge carriers. The corresponding false-color image of the PL spectrum intensity (Figure 2b) clearly demonstrates that the exciton peak is composed of two components, which are neutral exciton  $X_A$  and charged exciton  $X_A^-$  (also called trion) located at lower energy. The fitted energies and integrated intensities of  $X_A$  and  $X_A^-$  as a function of gate voltage are shown in Figure 2c,d. As the gate voltage increases, the intensity of neutral exciton  $X_A$  peak gradually decreases and nearly vanishes when the gate voltage exceeds  $25$  V. On the other hand, the trion  $X_A^-$  peak slowly becomes stronger from  $-40$  to  $0$  V and nearly keeps unchanged with the gate voltage further increasing, completely dominating



**Chunxiao Cong** received her B.Sc. degree in 2004 from Northeast Normal University (China), and then received her M.Sc. degree from Jilin University (China) in 2007. She received her Ph.D. degree in 2012 from Nanyang Technological University in Singapore. After a research fellowship at Nanyang Technological University in Singapore, she joined Fudan University as the National Thousand Youth Talents Plan Professor of China (2015). Prof. Chunxiao Cong's main research interests are optical and material properties of 2D layered materials and their applications in optoelectronics and flexible electronics.



**Jingzhi Shang** received both B.Sc. and M.Sc. degrees from Xiamen University (China) in 2006 and 2009, respectively. He then started to pursue his Ph.D. degree at Nanyang Technological University in Singapore. Since 2013 he is working as a research fellow in the same university. His current research interests are optical and material properties of 2D semiconductors.



**Yanlong Wang** received his Ph.D. degree in condensed-matter physics from Nanyang Technological University (NTU) in 2016. After working at NTU as a research staff for one year, he joined the Dalian Institute of Chemical Physics, Chinese Academy of Sciences as a researcher in 2017. He is currently interested in integrating optical thin films and 2D materials to achieve enhanced properties.

the positive voltage range. The gate-dependent peak intensities help identify the origin of trion to electron-bounded exciton because decrease in the electron concentration limits the formation of trion. In addition, the sample under  $0$  V is not in the insulating state, possibly due to the native doping caused by charge transfer from substrate.<sup>[19]</sup> The trion dissociation energy is defined as the minimum energy required for removing one electron from trion and could be calculated by the difference between the neutral exciton and trion. The trion dissociation energy increases from negative to positive

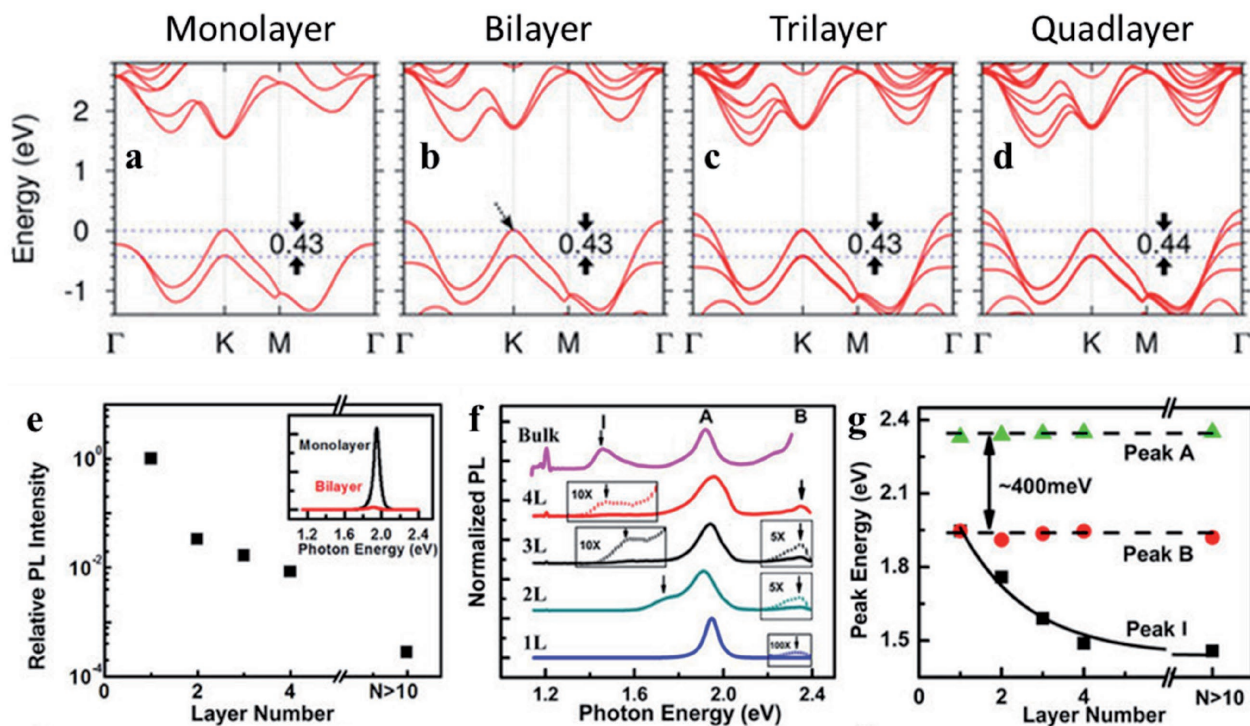


**Figure 1.** a–d) Band structure of WS<sub>2</sub> with different thicknesses. e) Thickness-dependent PL intensity of thin-layered WS<sub>2</sub>. The inset shows the comparison of PL spectra of 1L and bilayer WS<sub>2</sub>. f) Normalized PL spectra (by the intensity of A exciton peak) of WS<sub>2</sub> thin layers. g) The variations of energies of A, B, and I peaks with layer numbers. Reproduced with permission.<sup>[22]</sup> Copyright 2013, Nature Publishing Group.

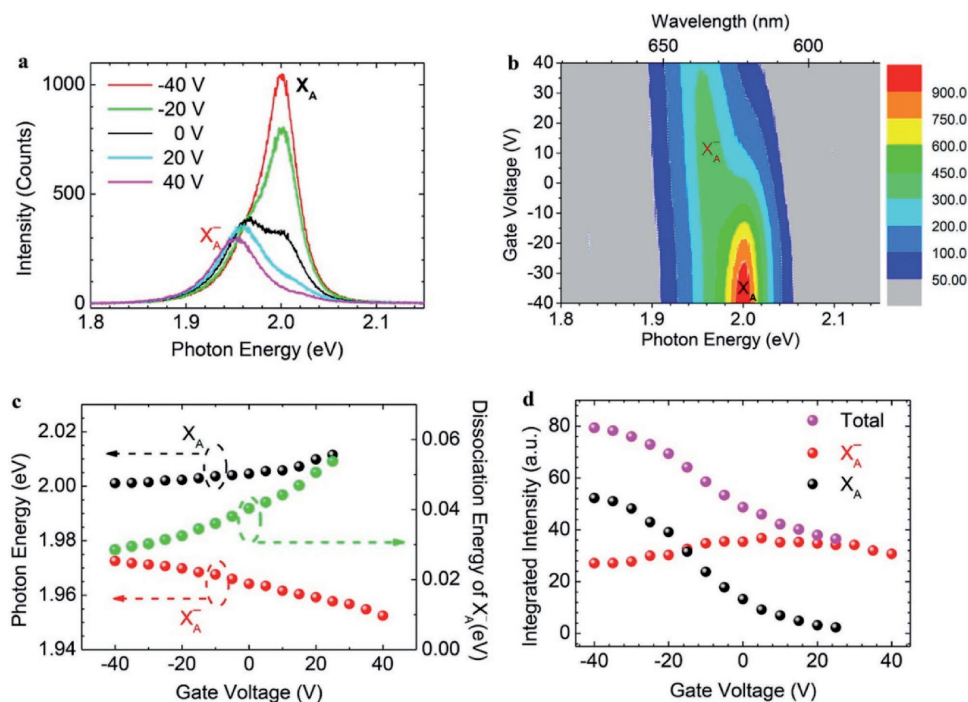


**Figure 2.** a) PL spectra and b) false-color image of the PL spectrum intensity as a function of gate voltage for 1L WS<sub>2</sub> at RT. c) The energies and d) integrated intensities of neutral and charged exciton extracted from the PL spectra of 1L WS<sub>2</sub> as a function of the gate voltage. Reproduced with permission.<sup>[27]</sup> Copyright 2015, American Chemical Society.



gate voltage (Figure 2c), which is attributed to the increase of Fermi level.<sup>[40]</sup>

### 2.1.2. Molecule Doping Effects

In addition to electrostatic gating, the charge transfer induced by molecule adsorption has also been shown to tune the Fermi level of 1L WS<sub>2</sub> by Peimyo et al.<sup>[34]</sup> It is demonstrated that 2,3,5,6-tetrafluoro-7,7,8,8-tetracyanoquinodimethane (also known as F4TCNQ) can withdraw electrons from 1L WS<sub>2</sub> and achieve p-type doping effect by electrical transport measurements.<sup>[34]</sup> As adsorption of the F4TCNQ increases, the intensity of the neutral exciton peak is significantly enhanced while that of negative trion slightly decreases in the first few steps and then remains stable in 1L WS<sub>2</sub> (Figure 3a,b). The observed trend is consistent with the evolution of PL features under negative electrostatic gate voltage and calculation results.<sup>[19,34]</sup> Moreover, the reversibly tunable exciton and trion by annealing effect has been studied by the same group (Figure 3c). After heat treatment, the spectral weight of neutral exciton is fully suppressed for F4TCNQ doped 1L WS<sub>2</sub>, which demonstrates the successful removal of the dopants. As a result, 1L WS<sub>2</sub> has a higher electron concentration after annealing and recovers its n-type conductivity. Redeposited by F4TCNQ molecule for the second round, the spectral weight of the neutral exciton increases and becomes larger compared with that of trion, indicating the reversible modulation of the exciton states in 1L WS<sub>2</sub> through the combination of molecule-doping and thermal annealing.

### 2.1.3. Strain Effects

The exceptionally high breaking strength of atomically thin layered materials provides a perfect platform for the implementation of strain engineering, which plays a crucial role in tuning properties of various 2D materials.<sup>[41–48]</sup> Wang et al. have applied uniaxial strain onto 1L WS<sub>2</sub> by elongating the flexible polyethylene terephthalate substrate and observed the tunable light emissions by in situ strained PL measurements.<sup>[35]</sup> Figure 4a displays the evolution of PL spectra in 1L WS<sub>2</sub> as a function of uniaxial strain. For lower strain less than 2.2%, the overall PL profile shows noticeable redshift with increasing strain. In the higher strain region more than 2.5%, a discernible PL peak broadening can be observed together with the further redshifts as the strain increases. This broadening is attributed to the additional contribution of light emission from the indirect optical transition (marked by I peak) and consistent with the calculated critical strain of around 2.6% which could induce the direct-indirect bandgap transition in 1L WS<sub>2</sub>.<sup>[35]</sup> From the fitted results in Figure 4b, strain can lead to the enhanced intensity of I peak, contrary to the rising trends of A and A<sup>-</sup> peaks. The coincident decrease of two intensity ratios, A<sup>-</sup>/I and A/I, shows direct-indirect spectral-weight transformation caused by increasing strain (Figure 4c), providing supplementary evidence for the assignment of I peak under higher strain. Figure 4d shows the fitted photon energies as a function of strain, and the slope of I peak ( $-0.0187$  eV %<sup>-1</sup>) is higher than those of A and A<sup>-</sup> peaks. Besides, the trion dissociation energy, defined as the energy difference between A and A<sup>-</sup> peaks, shows a decreasing trend with increasing uniaxial strain

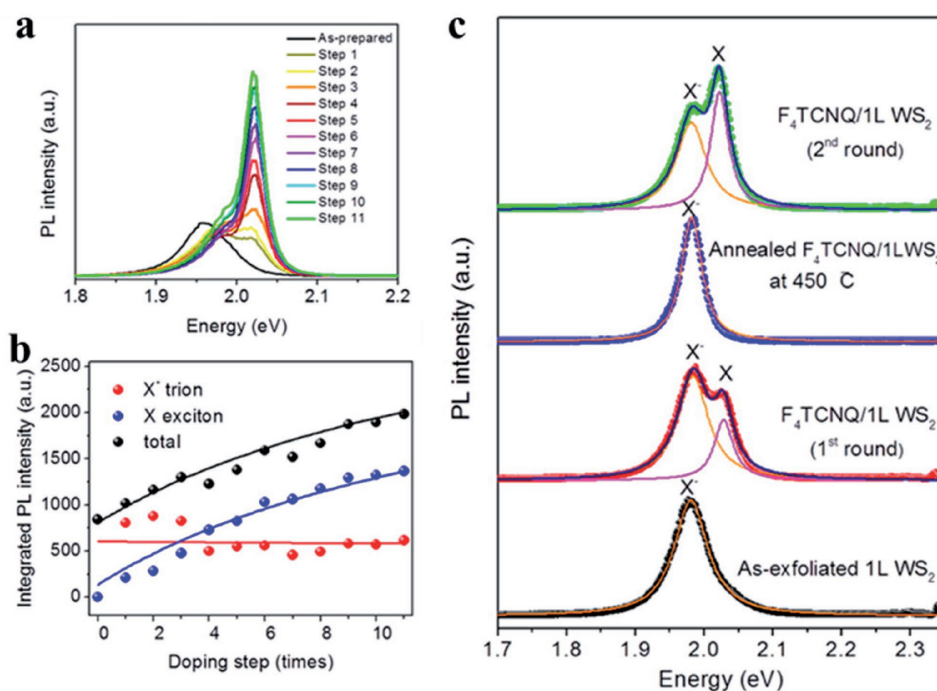


**Figure 3.** a) Comparison of PL spectra upon sequential doping with F4TCNQ for 1L WS<sub>2</sub> at RT. b) Integrated intensities of X, X<sup>-</sup>, and their sum after each doping step. Solid lines indicate the theoretical calculated PL intensities according to the rate equation. c) PL spectra of 1L WS<sub>2</sub>, 1L WS<sub>2</sub> doped by F4TCNQ, F4TCNQ/1L WS<sub>2</sub> after annealing, and F4TCNQ/1L WS<sub>2</sub> doped by second round of F4TCNQ. Reproduced with permission.<sup>[34]</sup> Copyright 2014, American Chemical Society.

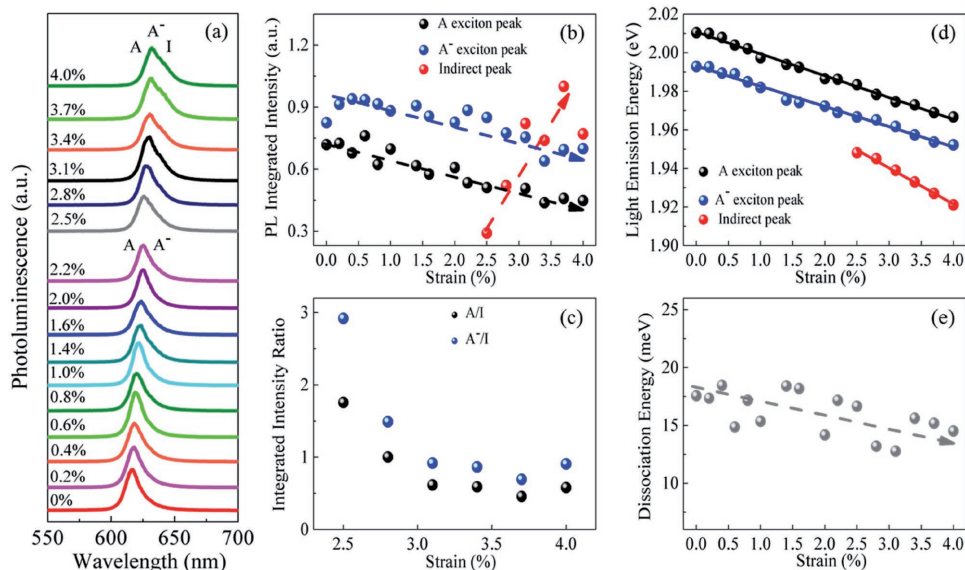


**Figure 4.** a) PL spectra, b) integrated intensities, and d) photon energies of different peaks for CVD-grown 1L WS<sub>2</sub> with increasing uniaxial strain. The integrated intensities of all peaks are normalized by the intensity of I peak under 3.7% strain. c,e) Integrated intensity ratios of direct-indirect transition peak and trion dissociation energies as a function of the strain, respectively. The dashed lines in (b) and (e) are used as guides for the corresponding trend under strain and the solid lines in (c) indicate the linear fitting. Reproduced with permission.<sup>[35]</sup> Copyright 2015, Tsinghua University Press and Springer-Verlag.

(Figure 4e), which can be well explained by the strain-induced modifications of polarizability and effective exciton mass.<sup>[49,50]</sup>

In addition, PL enhancement of multilayer WS<sub>2</sub> induced by local strain effect on WS<sub>2</sub> crystals has been reported by Dhakal et al.<sup>[51]</sup> In their work, the application of uniaxial strain was realized by generation of wrinkles on quad-layer WS<sub>2</sub>, as illustrated in Figure 5b. Local strain modifies the band structure of quad-layer WS<sub>2</sub>, in which  $\Lambda$ -conduction band valley (CBV) was aligned above the K-CBV (Figure 5a). As can be seen in Figure 5c, this indirect-direct bandgap crossover leads to the significant PL enhancement in the wrinkle region.<sup>[51]</sup>

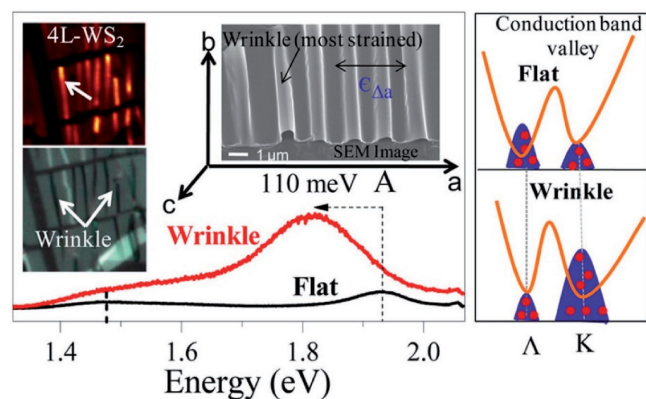


**Figure 5.** a) Calculated CBV of the unstrained and 2% strained quad-layer WS<sub>2</sub>. b) SEM image of the quad-layer WS<sub>2</sub> under uniaxial strain by way of wrinkle generation. c) PL spectra of the quad-layer WS<sub>2</sub> measured from the flat and wrinkled areas. The inset shows the PL spectral mapping and the optical image of the quad-layer WS<sub>2</sub> with the periodic wrinkle formation. Reproduced with permission.<sup>[51]</sup> Copyright 2017, American Chemical Society.

#### 2.1.4. Substrate Effects

Kobayashi et al. have investigated the substrate effects on the exciton properties in 1L WS<sub>2</sub>.<sup>[36]</sup> Figure 6a compares the PL spectra of chemical vapor deposition (CVD)-grown 1L WS<sub>2</sub> on four different substrates. The PL spectrum of WS<sub>2</sub> on graphite shows a symmetric profile dominated by the neutral exciton. In contrast, the PL spectra on *h*-BN, sapphire, and SiO<sub>2</sub>/Si can be fitted by two components of both neutral exciton and trion, which demonstrates the existence of local charge doping in these samples. 1L WS<sub>2</sub> samples on both graphite and *h*-BN exhibit narrow luminescence spectral width due to the lower defect concentrations and the weak light emission of 1L WS<sub>2</sub> on graphite is attributed to the fast nonradiative process in this sample.<sup>[36]</sup> To further understand the structural defects in WS<sub>2</sub> samples on different substrates, temperature dependence of PL spectra is compared on graphite and SiO<sub>2</sub>/Si substrates (Figure 6b,c). For both of the two samples, the overall PL profile redshifts with increasing temperature, which is a typical behavior of semiconductors.<sup>[52]</sup> In addition, it can be clearly seen that the PL profile of the WS<sub>2</sub> sample on graphite remains symmetric throughout the whole temperature range and its line width becomes sharper at lower temperature, reaching 8 meV at 79 K.<sup>[36]</sup> As to the sample on SiO<sub>2</sub>/Si, the linewidth does not show obvious temperature dependence and is still broad even at 79 K. These results suggest that graphite is an ideal substrate for the preparation of the high-quality WS<sub>2</sub> samples with extremely low doping concentration.<sup>[36]</sup>

#### 2.1.5. Valley Polarization

In addition to probing the effects of external perturbations on exciton properties, PL spectroscopy also serves as a powerful

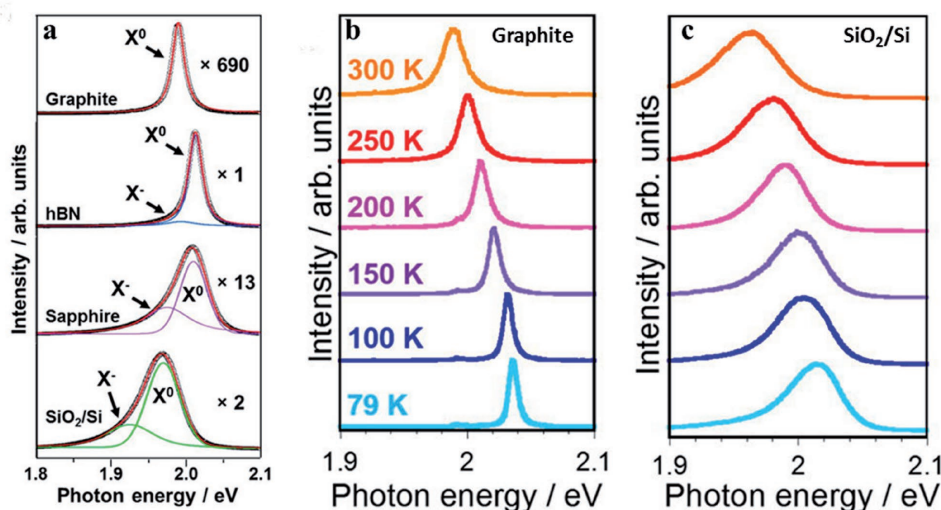


**Figure 6.** a) PL spectra of 1L WS<sub>2</sub> on SiO<sub>2</sub>/Si, sapphire, h-BN, and graphite substrates at RT. PL spectra of 1L WS<sub>2</sub> on b) graphite and c) SiO<sub>2</sub>/Si as a function of the temperature. Reproduced with permission.<sup>[36]</sup> Copyright 2015, American Chemical Society.

way to explore the valley physics in 1L WS<sub>2</sub>.<sup>[25,26,53]</sup> Valleytronics is a recent hot topic that makes use of the freedom degree of valley in electrons and has huge potential application prospects in the field of valleytronic devices. 1L WS<sub>2</sub> becomes a promising material for valleytronics because both of its valence and conduction band edges have two energy-degenerate valleys at *K* and *K'* points of the Brillouin zone.<sup>[53]</sup> Zhu et al. have systematically studied the circular dichroism of the exciton in 1L and bilayer WS<sub>2</sub>.<sup>[25]</sup> Figure 7a presents the circularly polarized PL spectra of 1L WS<sub>2</sub> under near-resonant excitation at 10 K. It is found that the PL spectrum is dominated by A exciton and the excited light inherits the circular polarization from that of excited light owing to the valley selection rules.<sup>[25]</sup> The degree of valley polarization is nearly constant throughout the energy range of A exciton and decays when the temperature increases, caused by the phonon-assisted electron scattering between

different valleys (Figure 7b). As shown in Figure 7c, the circular polarization is 16% at 10 K under the excitation energy of 2.33 eV, far away from the A exciton energy of 2.08 eV. This indicates that the off-resonance excitation also largely contributes to the depolarization process.<sup>[25]</sup>

#### 2.1.6. Plasmonic and Photonic Enhancement

The typical PL quantum yields of exfoliated and CVD-grown 1L WS<sub>2</sub> samples are relatively lower than presently well-developed III–V semiconductors, which limits their practical optoelectronic applications. Some efforts on PL enhancement have been made by introducing diverse plasmonic and photonic structures. Kern et al. have demonstrated the more than one order PL enhancement, the controllable polarization characteristics,

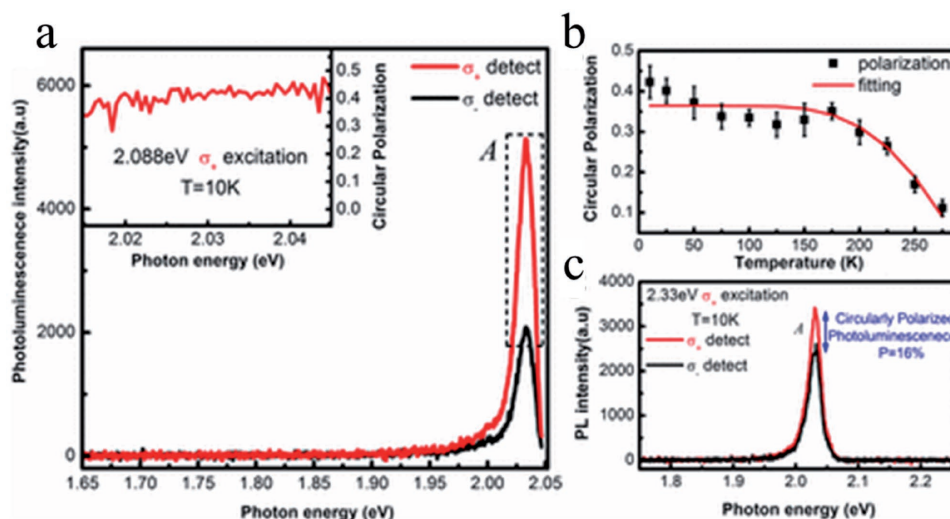


**Figure 7.** a) Circularly polarized PL spectra of 1L WS<sub>2</sub> with both  $\sigma_+$  and  $\sigma_-$  under near-resonant  $\sigma_+$  excitation at 10 K. The inset plots the degree of the valley polarization as a function of excitation energy. b) The temperature-dependent degree of the valley polarization for 1L WS<sub>2</sub>. c) Circularly polarized PL spectra under off-resonant excitation at 10 K. Reproduced with permission.<sup>[25]</sup> Copyright 2014, National Academy of Sciences.



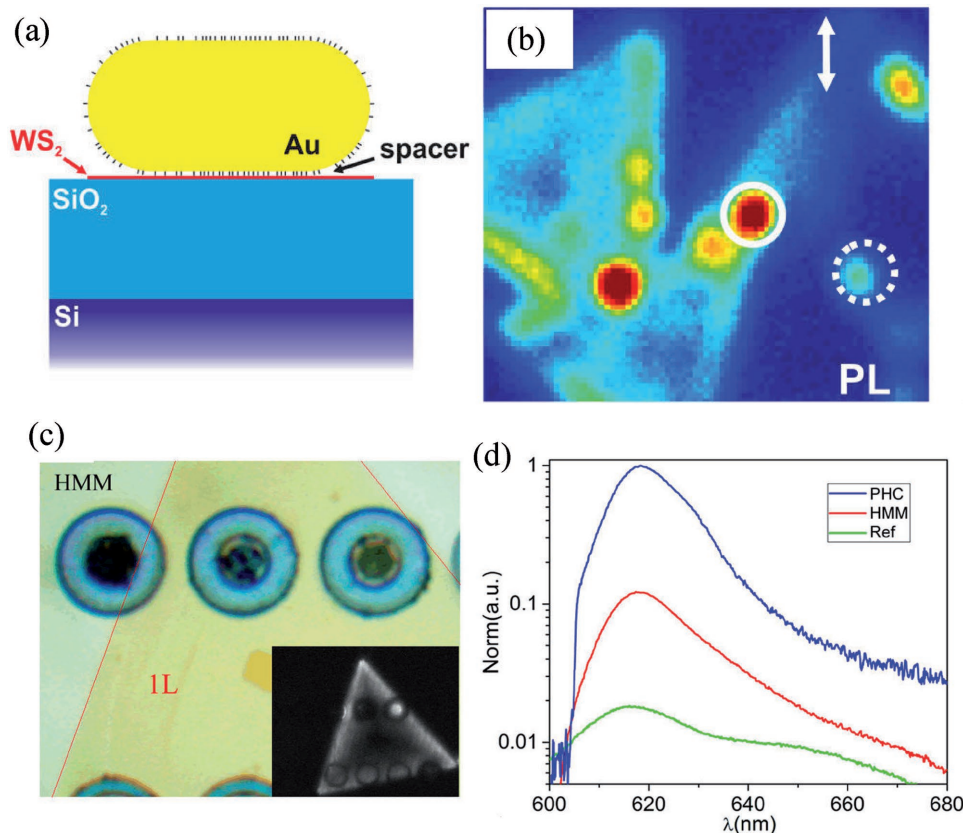


**Figure 8.** a) Schematic of the hybrid structure of Au-nanoantenna/1L WS<sub>2</sub>; b) PL intensity map of Au-nanoantenna/1L WS<sub>2</sub>; c) Optical image of 1L WS<sub>2</sub> flakes on photonic hypercrystals (PHC); d) PL emission spectra collected from three locations of 1L WS<sub>2</sub> on PHC, hyperbolic metamaterial (HMM), and Si. a,b) Reproduced with permission.<sup>[37]</sup> Copyright 2015, American Chemical Society. c,d) Reproduced with permission.<sup>[39]</sup> Copyright 2016, American Chemical Society.

and the modified spectral profiles of CVD-grown 1L WS<sub>2</sub> by use of gold nanoantennas (Figure 8a,b), which is strongly associated with the plasmonic resonance of nanoantennas.<sup>[37]</sup> Moreover, Ag films and nanowires together with the sapphire spacers have also been used to boost the PL of 1L WS<sub>2</sub> by the coupling between excitons and surface plasmon polaritons, where the optimal spacer thickness and the new composite system are important for the PL enhancement.<sup>[38]</sup> Interestingly, Galfsky et al. have reported the promising broadband enhancement via the photonic hypercrystals consisting of hyperbolic metamaterials and photonic crystal lattice, where the lifetime of the spontaneous exciton emission significantly reduces (Figure 8c,d).<sup>[39]</sup>

### 2.1.7. Defect Effects

Due to the inevitable existence of defects, the measured quantum yield in 2D WS<sub>2</sub> is quite poor.<sup>[32]</sup> Recently, Amani et al. have explored the effects of chemical treatment on defects and quantum yield in 1L WS<sub>2</sub>.<sup>[54]</sup> As shown in Figure 9, the quantum yield for 1L WS<sub>2</sub> after

chemical treatment by organic superacid bis(trifluoromethane) sulfonamide (TFSI) is significantly enhanced compared to the untreated sample and achieves near-unity at low pump power.

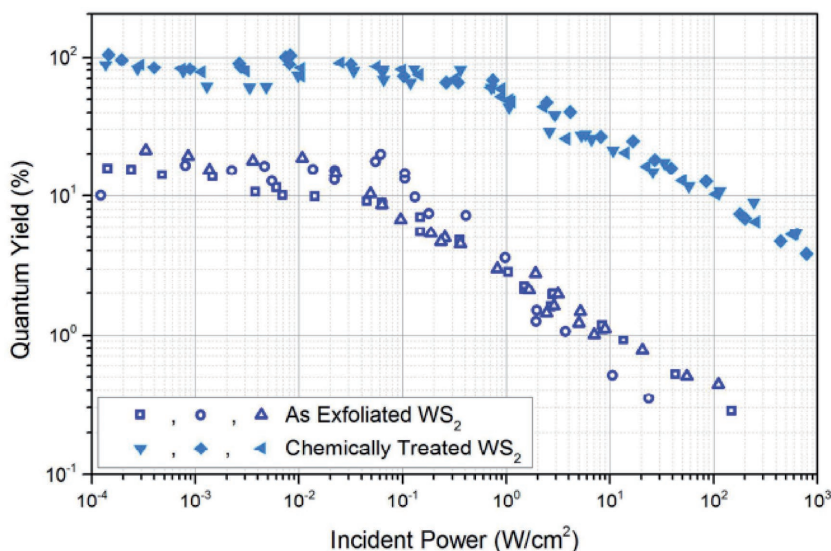


**Figure 9.** Incident power dependence of the quantum yield for several as-exfoliated and chemically treated monolayer WS<sub>2</sub> samples. Reproduced with permission.<sup>[54]</sup> Copyright 2016, American Chemical Society.

In the case of mechanically exfoliated 1L WS<sub>2</sub>, the dominant defect type is sulfur vacancies. This type of defect could be effectively repaired by TFSI treatment, which leads to the drastic increase of quantum yield.<sup>[54]</sup> For selenide-based TMDs, the same chemical treatment becomes ineffective because their defect types are more complex compared with WS<sub>2</sub>.

## 2.2. Bound Exciton

The existence of defects or impurities in the 2D materials could be bound with the excitons to form bound excitons, which allows for the detection of defects by defect-related spectral features.<sup>[33]</sup> Chow et al. investigated the effect of defects on PL features of 1L WS<sub>2</sub>.<sup>[55]</sup> It is found that a new PL peak (denoted as X<sup>D</sup>) appears at around 1.88 eV after ion bombardment treatments, which is attributed to defect-bounded excitons (Figure 10a). The spectral weight of this defect-related peak rises rapidly with increasing plasma treatment time, while the neutral exciton and trion peaks decrease obviously in weight. The origin of the defect-related peak was explored by examining the PL spectral features of the defective 1L WS<sub>2</sub> as a function of excitation power (Figure 10b,c).<sup>[55]</sup> The spectral weight of X<sup>D</sup> initially increases and then decreases with increasing laser power, which suggests the saturation of the defect site with the trapped excitons. The existence of the defect-related peak without remarkable contribution of the trion peak indicates that defect-bounded excitons are charge-free. Because the pristine sample free of defects does not display the X<sup>D</sup> peak despite having a large contribution of the trion feature, Chow et al. pointed out that the defect-related peak in PL originates from defect states which function as exciton traps instead of the radiative transitions related to the impurity levels.<sup>[55]</sup>

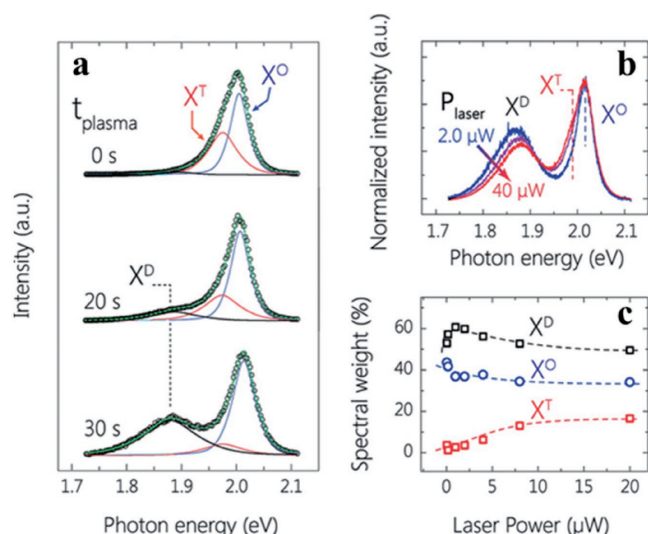


**Figure 10.** a) PL spectra of 1L WS<sub>2</sub> (normalized by the overall PL intensity) after sequential plasma treatment at RT. X<sup>O</sup>, X<sup>T</sup>, and X<sup>D</sup> indicate neutral, negatively charged, and defect-related exciton peaks, respectively. b) PL spectra and c) spectral weights of the different components for the defective 1L WS<sub>2</sub> as a function of excitation power. Reproduced with permission.<sup>[55]</sup> Copyright 2015, American Chemical Society.

## 2.3. Biexciton

Multiexcitons could be formed through the interaction between different excitons. Here, we give a brief review of biexciton in 1L WS<sub>2</sub>. Recently, Shang et al. have experimentally demonstrated the biexciton features of WS<sub>2</sub> by PL spectroscopy.<sup>[27]</sup> Figure 11a displays the evolution of PL spectra in 1L WS<sub>2</sub> as a function of laser excitation power at 4 K. Under relatively low excitation powers of 7 and 65 μW, only neutral exciton (X<sub>A</sub>), trion (X<sub>A</sub><sup>-</sup>), and localized states (LS) caused by defects appear in PL spectra of 1L WS<sub>2</sub>. One extra band denoted as X<sub>A</sub>X<sub>A</sub> appears near 1.98 eV under high excitation power of 9570 μW and is assigned as biexciton. The gradual evolution of the four spectral components with the laser excitation power could be more clearly seen in the false-color image of PL spectrum intensity versus photon energy and excitation power (Figure 11b). As shown in Figure 11c, X<sub>A</sub>X<sub>A</sub> peak slightly blueshifts with increasing excitation power, while the energies of neutral exciton and trion do not change much throughout the same power range, indicating the decrease of the dissociation energy of biexciton caused by higher excitation power. Remarkably, the intensity of the X<sub>A</sub>X<sub>A</sub> peak exhibits a superlinear behavior with  $\alpha$  value of around 1.9, in stark contrast to the sublinear behavior for LS and linear behaviors for X<sub>A</sub> and X<sub>A</sub><sup>-</sup> (Figure 11d). This provides strong evidence for the assignment of the X<sub>A</sub>X<sub>A</sub> peak.<sup>[27]</sup>

After the stimulating discovery of neutral and charged exciton with fascinating physics, researchers put biexciton in their wish list and successfully found the evidence to prove its existence in several 2D TMDs.<sup>[27,56,57]</sup> Biexcitons is a four-body state, comprising of two bound electron–hole pairs. When the exciton density increases with the fluence of excitation light, biexciton is predicted to form and could be identified by PL spectroscopy, with distinct spectroscopic feature with respect to neutral and charged exciton.<sup>[58]</sup> Through a cascade radiative process, each biexciton emits two photons with different energies. After emission of the first photon, the remaining exciton could emit the second photon with a higher energy than the first one. The energy difference is the gained energy when two excitons bind into a unity, the so-called biexciton binding energy.<sup>[58]</sup>

## 2.4. Spatial Characteristics of Exciton Complexes

The heterogeneous PL emission is frequently observed in 1L WS<sub>2</sub> crystals, especially for CVD-grown samples. Kim et al. have reported the distinct spatial patterns of PL features as a function of excitation laser power in CVD-grown 1L WS<sub>2</sub>.<sup>[59]</sup> Figure 12a displays the evolution of PL intensity and position images of 1L WS<sub>2</sub> with increasing laser power. It is found that the edges of triangle WS<sub>2</sub> grains exhibit much stronger light emission compared to the inner parts independent of laser power. In contrast, the PL position images are sensitive to the laser power. Under low laser power of around 0.3 μW, the overall PL peak of the edge has higher energy than that at the inner area, while the trend becomes opposite in the case of high laser power of around 100 μW. For the condition of intermediate power, the PL position image is uniform. To probe the origin of the dependence of observed spatial characteristics on laser power, the PL spectra obtained from the edge and inner



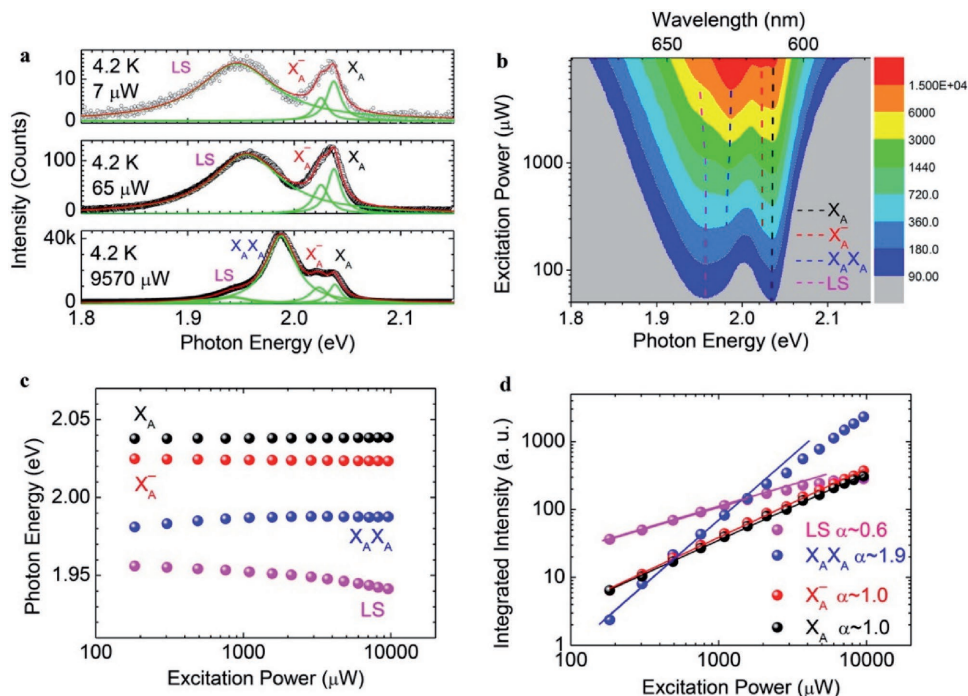


**Figure 11.** a) The evolution of PL spectra of 1L WS<sub>2</sub> as a function of excitation powers at 4.2 K. b) False-color image of the PL spectrum intensity as a function of photon energy and excitation power. The dashed curves act as guide lines to indicate the spectral evolution. c) Photon energies and d) intensities of four spectral components versus excitation laser power. The solid lines in (d) show the linear fitting and the  $\alpha$  value is the slope of each spectral component. Reproduced with permission.<sup>[27]</sup> Copyright 2015, American Chemical Society.

areas for each laser power were fitted by neutral excitons ( $A^0$ ), trions ( $A^-$ ), and biexcitons ( $AA$ ). As can be seen from the fitted results in Figure 12b,c, the biexciton peak does not contribute to the PL spectra of 1L WS<sub>2</sub> in the inner regions, but completely dominates the PL emission from the edge regions under high excitation power. The predominant emission comes from  $A^-$  and  $A^0$  throughout the whole power range in the inner regions, but the governed exciton changes as the power varies in edge regions and maintains the stronger PL intensities compared to the inner regions. The more intense PL emission and larger variation of exciton-type contribution in the edges of triangle 1L WS<sub>2</sub> grains is attributed to the larger concentration of electrons, which facilitates the formation of various exciton complexes including neutral exciton, trion, and biexciton.<sup>[59]</sup>

### 3. Luminescence beyond Fundamental Excitonic Emission of 2D WS<sub>2</sub>

#### 3.1. Single-Photon Emission

Single-photon sources are important for the next-generation quantum information and communications. Recently, the rising 2D semiconductors have become the new candidates for preparing on-chip single photon emitters.<sup>[60–63]</sup> On-demand single photon emitters generally request high purity, excellent indistinguishability, large generation, and extraction efficiencies. More practically, the room-temperature operation and electrical pumping are preferred for the practical on-chip quantum technologies. As shown in previous studies,<sup>[60–63]</sup> the

bound excitons and/or defect-related emission exist in typical exfoliated and CVD-grown 1L WS<sub>2</sub>, which could be the potential single-photon sources after additional design and engineering. Palacios-Berraquero et al. have reported deterministic single-photon arrays of 1L WS<sub>2</sub> enabled by silica nanopillars and the cryogenic environment (Figure 13).<sup>[29]</sup> Toward the on-chip quantum light applications, further investigation can be extended to optimization of operation temperature, improvement of the single-photon purity and efficiency, controllable manipulation of quantum entanglement, and development of integration strategies with conventional semiconductor fabrication processes.

#### 3.2. Exciton–Polaritons

In general, the coupling between excitons and photons can result in the formation of exciton–polaritons. One efficient strategy to obtain exciton–polaritons is employing the planar semiconductor microcavity, where the designed cavity photon can strongly couple with the excitonic emission bands and give rise to the so-called microcavity polaritons featured by the split upper and lower polariton branches. The fundamentally attracting properties are expected to be observed at room temperature in such 2D semiconductor based on polaritonic systems such as Bose–Einstein condensation, superfluidity, superconductivity, and other strong nonlinearities. The intrinsically large exciton binding energy of 1L WS<sub>2</sub> is in favor of stable exciton–polariton at room temperature, which is superior to most counterparts based on conventional semiconductors

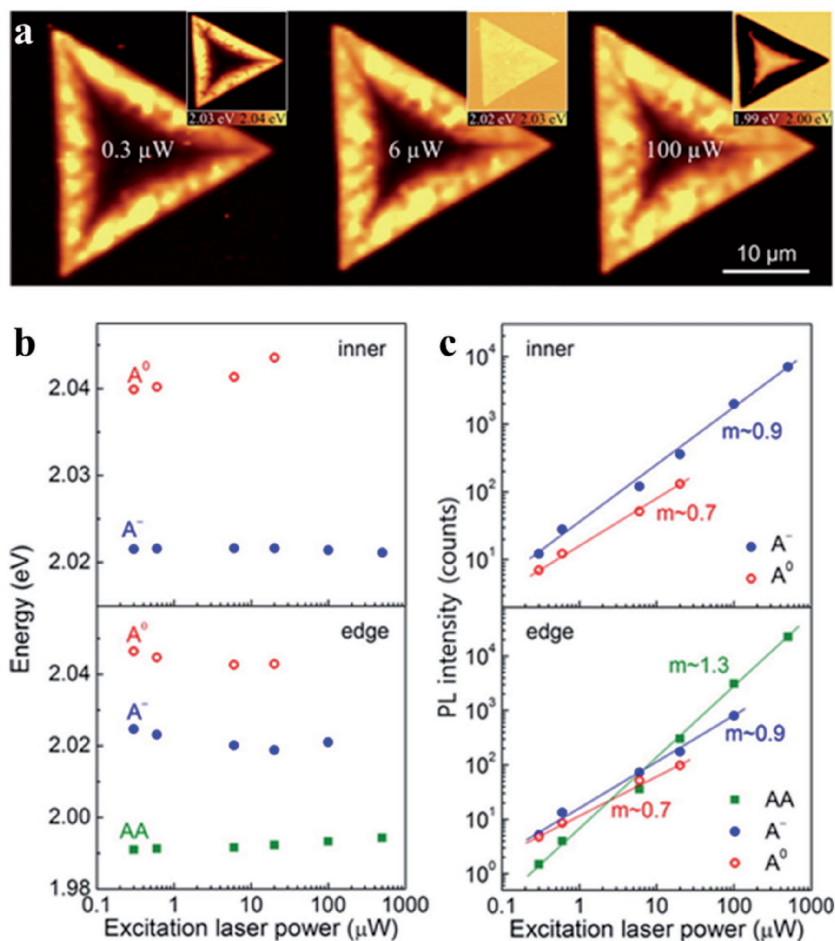


**Figure 12.** a) PL intensity images of 1L WS<sub>2</sub> with increasing laser power. The insets show the PL position images of the same sample corresponding to each laser power. b) Fitted energies and c) intensities of different PL peaks as a function of incident laser power. The solid lines denote power law fits and the values of  $m$  indicate the numeric power. Reproduced with permission.<sup>[59]</sup> Copyright 2016, American Chemical Society.

in view of developing practical applications. Flatten et al. have reported the exciton–polariton formation of 1L WS<sub>2</sub>-coupled open microcavity (Figure 14)<sup>[30]</sup> and electrically tunable hybrid polaritons in a 1L WS<sub>2</sub>-dye embedded microcavity<sup>[64]</sup> together with the large Rabi splitting and the mixed excitonic nature. Further investigation can be extended to the experimental exploration of the possible room-temperature superfluidity, superconductivity, and low threshold polariton lasing, where the rich many body physics can be explored such as quantized vortices, quantum phases, and polaritonic coherence properties.

### 3.3. Stimulated Emission

To develop the promising optical interconnects and quantum communications, the on-chip coherent light sources are highly demanded and the emerging material system of direct bandgap 2D semiconductors opens up new opportunities. In general, the resonant optical cavity is requested to enhance the spontaneous emission rate and further realize the stimulated emission. As a consequence, the lasing light from such photonic devices containing the gain media of 2D semiconductors can be obtained. 1L WSe<sub>2</sub> and WS<sub>2</sub> lasing devices by use of the photonic crystal cavity<sup>[65]</sup> and the microdisk,<sup>[31]</sup> respectively, have been realized at cryogenic temperatures, where the high quality factors and the relatively high quantum yield play important role in reducing the thresholds.

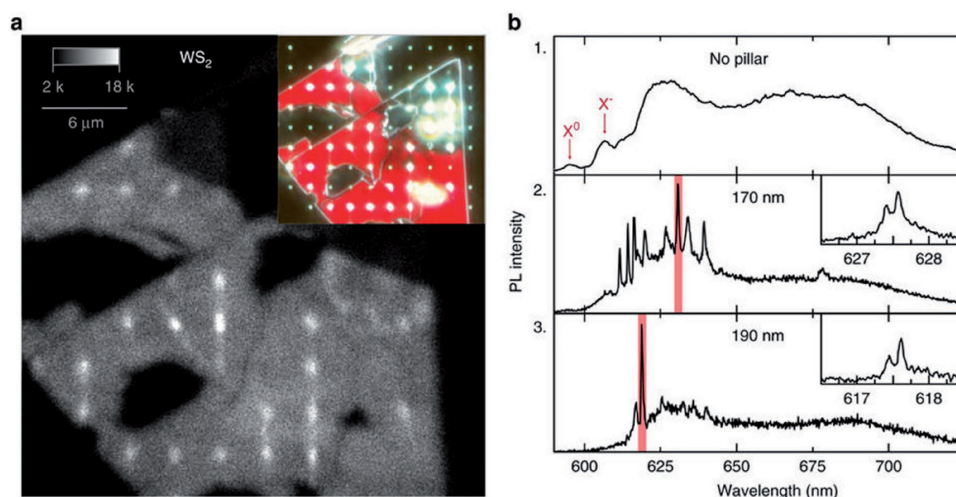


**Figure 13.** a) PL intensity map of a 1L-WS<sub>2</sub> on nanopillar arrays collected at 10 K. b) PL spectra of 1L-WS<sub>2</sub> regions located at the flat substrate, 170 and 190 nm pillars, respectively. Reproduced with permission.<sup>[29]</sup> Copyright 2017, Nature Publishing Group.

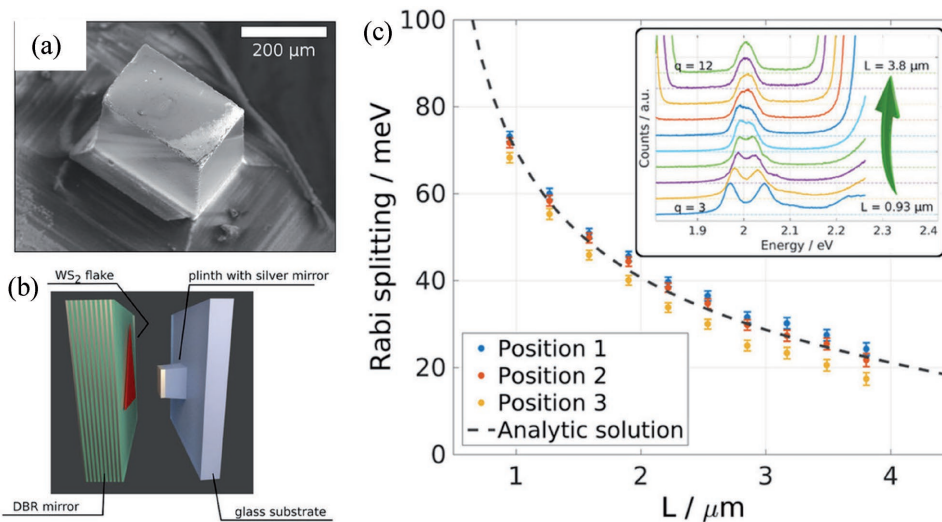


**Figure 14.** a) Image of Ag on the silica plinth; b) schematic of a 1L WS<sub>2</sub> open cavity; c) Rabi-splitting versus cavity length. Inset shows transmission spectra of the cavities with different cavity lengths; Reproduced with permission.<sup>[30]</sup> Copyright 2016, Nature Publishing Group.

Meanwhile, a multimode lasing device of few-layer MoS<sub>2</sub> has been demonstrated by employing a hybrid microsphere-micro-disk cavity, which operates at room temperature and presents a low threshold under continuous wave photoexcitation.<sup>[66]</sup> To further realize the practical 1L semiconductor lasing applications, the further development of electrically driven lasing devices and their on-chip arrays is highly demanded.

### 3.4. Electroluminescence

Generation of electroluminescence from a 2D semiconductor is very important to further develop the practical light-emitting devices. Sundaram et al. have reported the electroluminescence from 1L MoS<sub>2</sub> field-effect transistor, where the emission mechanism is attributed to a hot carrier process occurring around the metal-MoS<sub>2</sub> contact region.<sup>[67]</sup> Moreover, the electroluminescence has also been demonstrated in p-n heterojunctions containing the hole-doped bulk silicon and the electron-doped MoS<sub>2</sub>, where the emission species of excitons, trions, and bound excitons may take responsibilities.<sup>[68,69]</sup> In particular, the typical 1L TMDs such as 1L WS<sub>2</sub> and WSe<sub>2</sub> own the unique valley degree associated with the inversion symmetry breaking, which allows developing the chiral electroluminescence. Zhang et al. have observed the circularly polarized electroluminescence from 1L and few-layer WSe<sub>2</sub> by using electric-double-layer transistor structures and the gated ionic liquid.<sup>[70]</sup> More importantly, toward the practical light-emitting devices, the mass production is generally required and the large-area samples grown by chemical vapor deposition can enable such scalable applications. Electrically tunable valley-polarized light-emitting diode has been demonstrated at cryogenic temperatures in a p-i-n heterojunction consisting of p-type Si, CVD-grown 1L WS<sub>2</sub>, and n-type ITO, respectively (Figure 15).<sup>[71]</sup> Further studies on improvement of the electroluminescence quantum efficiency and room temperature operation will be very helpful for feasible 2D-semiconductor LED applications.

### 3.5. Harmonic Generation

Nonlinear optical properties of 1L TMDs have been investigated under high-intensity laser excitations, implying the promising photonic applications for strong and high harmonic generations.<sup>[72–77]</sup> Owing to the broken inversion symmetry in 1L WS<sub>2</sub>, the intense second harmonic generation has been uncovered, where the extracted second-order nonlinear susceptibility is more than 100 times of that of a conventional nonlinear crystal (BBO).<sup>[75]</sup> Moreover, the second harmonic generation shows the clear layer number dependence and the generated second harmonic signals in odd layers present the larger efficiencies than the ones of even layers reflecting the change of the structural inversion symmetry.<sup>[74]</sup> The third-order nonlinearities of mono- and few-layer WS<sub>2</sub> have been explored by the two wave mixing technique, where the optical Kerr effect plays an important role.<sup>[78]</sup> The strong harmonic generation properties enable the nonlinear microscopic investigation of these layered materials with the significantly enhanced contrast and the reduction of the potential substrate-induced light interference and such nonlinear optical microscopic approaches can be used to probe the diverse properties associated with structural symmetries such as thicknesses, orientations, edges, stacking orders, grain boundaries, and sizes of these layered crystals and their heterostructures.<sup>[73,79]</sup>

### 3.6. Dark Excitons

Dark excitons consisting of electron-hole pairs with parallel spins have been revealed in 1L TMDs, which are strongly related to the splitting electronic structures around both valance and conduction band edges resulted from strong spin-orbit coupling (Figure 16a).<sup>[80–87]</sup> The lowest transition of the intravalley A exciton in an ideal 1L WS<sub>2</sub> is optically dark according to electron and hole spin configurations.<sup>[81,82,85]</sup> The dark A exciton of 1L WS<sub>2</sub> has been observed under the in-plane



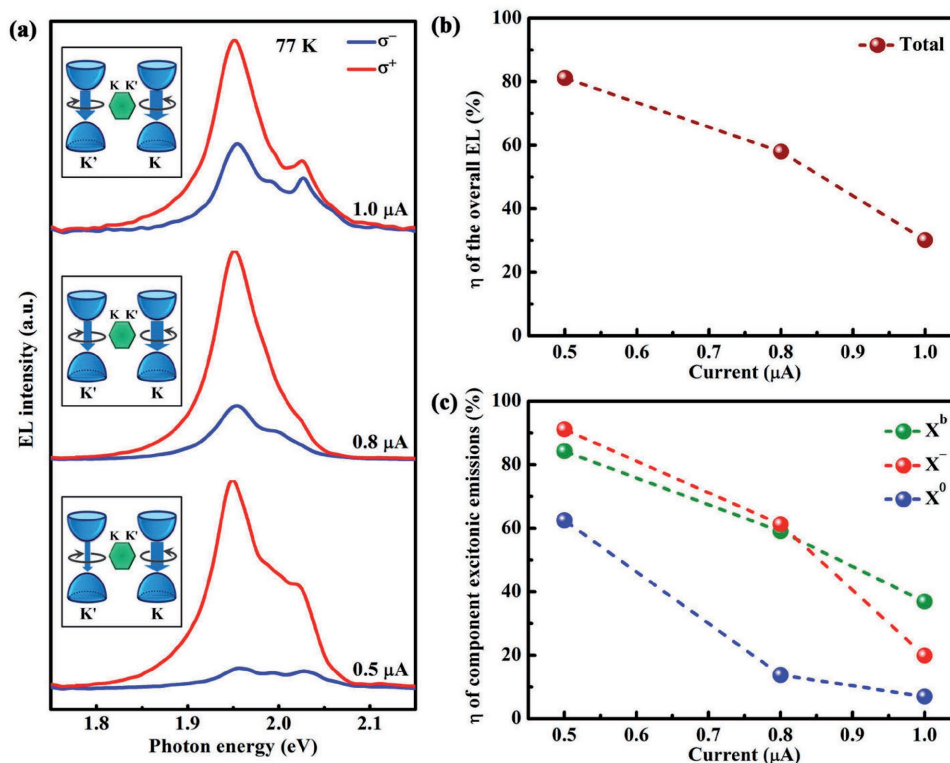


**Figure 15.** a) The current dependent electroluminescence spectra.  $\sigma_+$  and  $\sigma_-$  represent right-handed circular electroluminescence components, respectively. Insets show the schematics of valley-contrasting circular dichroism. b, c) Current dependences of the total emission and three components of neutral exciton ( $X^0$ ), negative trion ( $X^-$ ), and bound exciton ( $X^b$ ). Reproduced with permission.<sup>[71]</sup> Copyright 2016, American Chemical Society.

magnetic field of 14 T at 4.2 K (Figure 16b), which is located at 47 meV below the emission energy of A exciton.<sup>[81]</sup> The dark exciton states at higher excited states have also been observed in 1L WS<sub>2</sub> at the excitation wavelength of 990 nm and 10 K via two-photon excitation spectroscopy.<sup>[80]</sup> Moreover, dark trions and biexcitons have also been predicted in 1L WS<sub>2</sub>, which can be optical bright by introducing the intervalley electron and electron scattering.<sup>[88]</sup> Furthermore, Danovich et al. have suggested that Auger recombination processes of dark excitons may take responsibilities for the low PL quantum efficiency of 1L WS<sub>2</sub>.<sup>[89]</sup> Technically, one promising application of such dark excitons with long lifetimes in such 1L TMDs is to form the coherent two-level system for quantum information.

### 3.7. Exciton Dynamics

Investigation of exciton dynamics is important for understanding fundamental optical properties of 1L WS<sub>2</sub> and developing practical optoelectronic devices such as low quantum yield, intervalley scattering, and light-emitting diodes. Ultra-short exciton formation time (<1 ps) has been estimated by analyzing the decay signals under ultrafast resonant and non-resonant excitations.<sup>[90]</sup> Moreover, exciton valley relaxation between K and K' valleys has been determined in 1L WS<sub>2</sub> by monitoring the decay of the circular polarization anisotropy, where fast (<1 ps) and slow valley relaxation times have been extracted for electrons and holes, respectively.<sup>[91]</sup> Strong

Coulomb-induced intervalley scattering plays an important role in the decay of the valley polarization and also results in the bandgap renormalization together with the dispersive signals in the transient absorption measurement.<sup>[92]</sup> More interestingly, comparable time-resolved Kerr rotation measurements have been performed for tungsten- and molybdenum-based 1L TMDs, where the additional long-lived time component has been observed for 1L WS<sub>2</sub> and attributed to optically dark excitons.<sup>[93]</sup> In particular, exciton recombination kinetics of as-exfoliated 1L WS<sub>2</sub>, chemically treated samples with high quantum yields, and encapsulated 1L WS<sub>2</sub> has been investigated, where the radiative decays strongly depend on the excitation powers, the defect passivation, dielectric surroundings, and exciton-exciton annihilation.<sup>[94,95]</sup> Besides, the diffusion dynamics of both neutral and charged excitons has also been investigated at varied temperatures in 1L WS<sub>2</sub> and the extracted exciton diffusion lengths have been affected by different mechanisms such as thermal activation and scattering processes involved with impurities, optical and acoustic phonons.<sup>[96]</sup>

## 4. Summary and Outlook

To sum up, we have discussed the interesting optical properties of the emerging 2D semiconductor of 1L WS<sub>2</sub> with the diverse excitonic states and modified excitonic emission. The large excitonic effects in 1L WS<sub>2</sub> greatly enable the room-temperature investigation of excitonic properties and development of

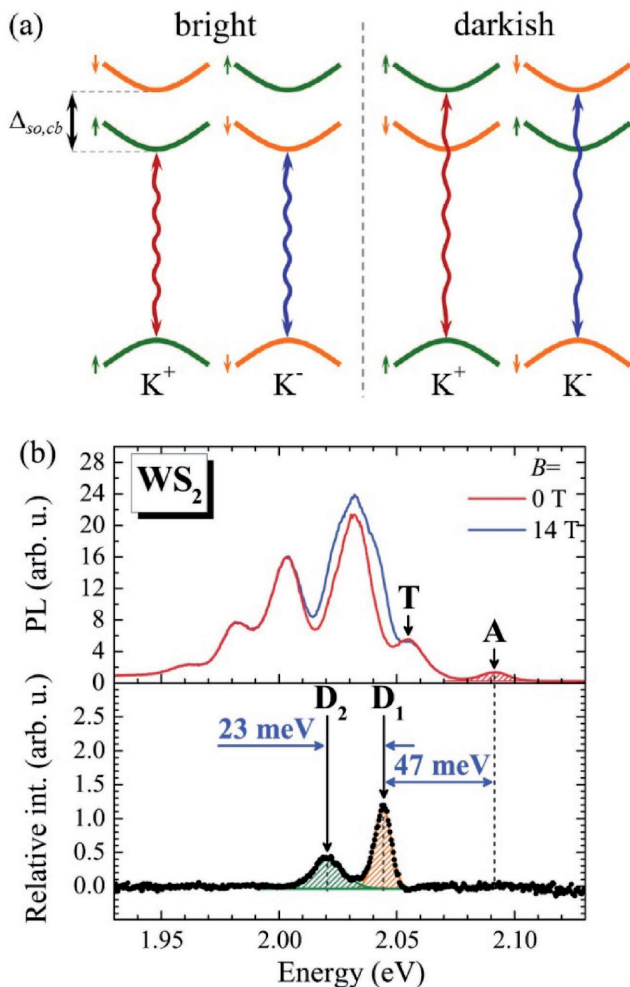


**Figure 16.** a) Diagram of relevant sub-bands in the conduction and valance bands at the  $K$  and  $K'$  points of the Brillouin zone in the bright and darkish 1L TMDs. The green (orange) curves indicate the spin-up (spin-down) sub-bands. The red and blue wavy lines show the A exciton transitions which are optically active.  $\Delta_{so,cb}$  denotes the spin-orbit splitting in the conduction band. b) PL spectra of 1L  $WS_2$  at  $T = 4.2$  K measured at zero field (red curves) and at  $B = 14$  T (blue curves) applied in the plane of the crystal. Reproduced with permission.<sup>[81]</sup> Copyright 2017, IOP Publishing.

excitonic optoelectronic devices. With the proper material engineering such as doping and strain, the widely tunable optical properties can be obtained. In the view of the large-scale material preparation, the crystal quality and the sample uniformity of the grown 1L  $WS_2$  samples are still needed to be improved in order to obtain higher luminescence quantum yields and stable emission features. Further optical investigation of 1L  $WS_2$  can be extended to higher-order multiple excitonic states,<sup>[97]</sup> plexcitons,<sup>[98,99]</sup> Bose-Einstein condensate states,<sup>[100]</sup> superfluidity,<sup>[101]</sup> and other many body physics. The future development of 2D-semiconductor based quantum emitters and exciton-polariton lasers under electrical injection and at room temperature could open up new opportunities for the promising on-chip and room-temperature optical interconnects, quantum information, and computing.

## Acknowledgements

This work was mainly supported by the National Young 1000 Talent Plan of China, the Shanghai Municipal Natural Science Foundation (No. 16ZR1402500), and Singapore MOE Tier 1 RG100/15.

## Conflict of Interest

The authors declare no conflict of interest.

## Keywords

2D semiconductors, 2D transition metal dichalcogenides, optical properties, tungsten disulfide

Received: July 20, 2017  
Revised: August 29, 2017  
Published online:

- [1] K. S. Novoselov, A. K. Geim, S. V. Morozov, D. Jiang, Y. Zhang, S. V. Dubonos, I. V. Grigorieva, A. A. Firsov, *Science* **2004**, *306*, 666.
- [2] K. S. Novoselov, A. K. Geim, S. V. Morozov, D. Jiang, M. I. Katsnelson, I. V. Grigorieva, S. V. Dubonos, A. A. Firsov, *Nature* **2005**, *438*, 197.
- [3] Y. Zhang, Y.-W. Tan, H. L. Stormer, P. Kim, *Nature* **2005**, *438*, 201.
- [4] A. H. Castro Neto, F. Guinea, N. M. R. Peres, K. S. Novoselov, A. K. Geim, *Rev. Mod. Phys.* **2009**, *81*, 109.
- [5] H. Zeng, X. Cui, *Chem. Soc. Rev.* **2015**, *44*, 2629.
- [6] X. Huang, Z. Zeng, H. Zhang, *Chem. Soc. Rev.* **2013**, *42*, 1934.
- [7] X. Duan, C. Wang, A. Pan, R. Yu, X. Duan, *Chem. Soc. Rev.* **2015**, *44*, 8859.
- [8] H. Wang, H. Yuan, S. S. Hong, Y. Li, Y. Cui, *Chem. Soc. Rev.* **2015**, *44*, 2664.
- [9] Q. H. Wang, K. Kalantar-Zadeh, A. Kis, J. N. Coleman, M. S. Strano, *Nat. Nanotechnol.* **2012**, *7*, 699.
- [10] H. Schmidt, F. Giustiniano, G. Eda, *Chem. Soc. Rev.* **2015**, *44*, 7715.
- [11] F. Xia, H. Wang, D. Xiao, M. Dubey, A. Ramasubramaniam, *Nat. Photonics* **2014**, *8*, 899.
- [12] M. Chhowalla, H. S. Shin, G. Eda, L.-J. Li, K. P. Loh, H. Zhang, *Nat. Chem.* **2013**, *5*, 263.
- [13] K. F. Mak, J. Shan, *Nat. Photonics* **2016**, *10*, 216.
- [14] W. Xu, W. Liu, J. F. Schmidt, W. Zhao, X. Lu, T. Raab, C. Diederichs, W. Gao, D. V. Seletskiy, Q. Xiong, *Nature* **2017**, *541*, 62.
- [15] H. Hong, C. Liu, T. Cao, C. Jin, S. Wang, F. Wang, K. Liu, *Adv. Mater. Interfaces* **2017**, *4*, 1601054.
- [16] F. Liu, J. Zhou, C. Zhu, Z. Liu, *Adv. Funct. Mater.* **2017**, *27*, 1602404.
- [17] J. van den Brink, *Nat. Mater.* **2010**, *9*, 291.
- [18] L. Yuan, L. Huang, *Nanoscale* **2015**, *7*, 7402.
- [19] B. Zhu, X. Chen, X. Cui, *Sci. Rep.* **2015**, *5*, 9218.
- [20] Z. Ye, T. Cao, K. O'Brien, H. Zhu, X. Yin, Y. Wang, S. G. Louie, X. Zhang, *Nature* **2014**, *513*, 214.
- [21] N. Peimyoo, J. Shang, C. Cong, X. Shen, X. Wu, E. K. L. Yeow, T. Yu, *ACS Nano* **2013**, *7*, 10985.
- [22] H. Zeng, G. B. Liu, J. Dai, Y. Yan, B. Zhu, R. He, L. Xie, S. Xu, X. Chen, W. Yao, X. Cui, *Sci. Rep.* **2013**, *3*, 1608.
- [23] H. R. Gutierrez, N. Perea-Lopez, A. L. Elias, A. Berkdemir, B. Wang, R. Lv, F. Lopez-Urias, V. H. Crespi, H. Terrones, M. Terrones, *Nano Lett.* **2013**, *13*, 3447.
- [24] H. Yu, X. Cui, X. Xu, W. Yao, *Natl. Sci. Rev.* **2015**, *2*, 57.

- [25] B. Zhu, H. Zeng, J. Dai, Z. Gong, X. Cui, *Proc. Natl. Acad. Sci. USA* **2014**, *111*, 11606.
- [26] P. K. Nayak, F.-C. Lin, C.-H. Yeh, J.-S. Huang, P.-W. Chiu, *Nanoscale* **2016**, *8*, 6035.
- [27] J. Shang, X. Shen, C. Cong, N. Peimyoo, B. Cao, M. Eginligil, T. Yu, *ACS Nano* **2015**, *9*, 647.
- [28] G. Plechinger, P. Nagler, J. Kraus, N. Paradiso, C. Strunk, C. Schüller, T. Korn, *Phys. Status Solidi RRL* **2015**, *9*, 457.
- [29] C. Palacios-Berraquero, D. M. Kara, A. R.-P. Montblanch, M. Barbone, P. Latawiec, D. Yoon, A. K. Ott, M. Loncar, A. C. Ferrari, M. Atatüre, *Nat. Commun.* **2017**, *8*, 15093.
- [30] L. C. Flatten, Z. He, D. M. Coles, A. A. Trichet, A. W. Powell, R. A. Taylor, J. H. Warner, J. M. Smith, *Sci. Rep.* **2016**, *6*, 33134.
- [31] Y. Ye, Z. J. Wong, X. Lu, X. Ni, H. Zhu, X. Chen, Y. Wang, X. Zhang, *Nat. Photonics* **2015**, *9*, 733.
- [32] W. Zhao, Z. Ghorannevis, L. Chu, M. Toh, C. Kloc, P.-H. Tan, G. Eda, *ACS Nano* **2012**, *7*, 791.
- [33] M. D. Tran, J.-H. Kim, Y. H. Lee, *Curr. Appl. Phys.* **2016**, *16*, 1159.
- [34] N. Peimyoo, W. Yang, J. Shang, X. Shen, Y. Wang, T. Yu, *ACS Nano* **2014**, *8*, 11320.
- [35] Y. Wang, C. Cong, W. Yang, J. Shang, N. Peimyoo, Y. Chen, J. Kang, J. Wang, W. Huang, T. Yu, *Nano Res.* **2015**, *8*, 2562.
- [36] Y. Kobayashi, S. Sasaki, S. Mori, H. Hibino, Z. Liu, K. Watanabe, T. Taniguchi, K. Suenaga, Y. Maniwa, Y. Miyata, *ACS Nano* **2015**, *9*, 4056.
- [37] J. Kern, A. Trügler, I. Niehues, J. Ewering, R. Schmidt, R. Schneider, S. Najmaei, A. George, J. Zhang, J. Lou, *ACS Photonics* **2015**, *2*, 1260.
- [38] F. Cheng, A. D. Johnson, Y. Tsai, P.-H. Su, S. Hu, J. G. Ekerdt, C.-K. Shih, *ACS Photonics* **2017**, *4*, 1421.
- [39] T. Galfsky, Z. Sun, C. R. Consideine, C.-T. Chou, W.-C. Ko, Y.-H. Lee, E. E. Narimanov, V. M. Menon, *Nano Lett.* **2016**, *16*, 4940.
- [40] K. F. Mak, K. He, C. Lee, G. H. Lee, J. Hone, T. F. Heinz, J. Shan, *Nat. Mater.* **2013**, *12*, 207.
- [41] D. Akinwande, N. Petrone, J. Hone, *Nat. Commun.* **2014**, *5*, 5678.
- [42] H.-Y. Chang, S. Yang, J. Lee, L. Tao, W.-S. Hwang, D. Jena, N. Lu, D. Akinwande, *ACS Nano* **2013**, *7*, 5446.
- [43] R. Roldán, A. Castellanos-Gomez, E. Cappelluti, F. Guinea, *J. Phys.: Condens. Matter* **2015**, *27*, 313201.
- [44] Y. Wang, C. Cong, C. Qiu, T. Yu, *Small* **2013**, *9*, 2857.
- [45] Y. Wang, C. Cong, R. Fei, W. Yang, Y. Chen, B. Cao, L. Yang, T. Yu, *Nano Res.* **2015**, *8*, 3944.
- [46] M. Huang, H. Yan, C. Chen, D. Song, T. F. Heinz, J. Hone, *Proc. Natl. Acad. Sci. USA* **2009**, *106*, 7304.
- [47] T. Mohiuddin, A. Lombardo, R. Nair, A. Bonetti, G. Savini, R. Jalil, N. Bonini, D. Basko, C. Galotis, N. Marzari, K. Novoselov, A. Geim, A. Ferrari, *Phys. Rev. B* **2009**, *79*, 205433.
- [48] S. Yang, C. Wang, H. Sahin, H. Chen, Y. Li, S. S. Li, A. S. S. Peeters, Q. Liu, J. Li, S. Tongay, *Nano Lett.* **2015**, *15*, 1660.
- [49] L. Wang, A. Kutana, B. I. Yakobson, *Ann. Phys.* **2014**, *526*, L7.
- [50] T. C. Berkelbach, M. S. Hybertsen, D. R. Reichman, *Phys. Rev. B* **2013**, *88*, 045318.
- [51] K. P. Dhakal, S. Roy, H. Jang, X. Chen, W. S. Yun, H. Kim, J. Lee, J. Kim, J.-H. Ahn, *Chem. Mater.* **2017**, *29*, 5124.
- [52] M. Cardona, T. A. Meyer, M. L. Thewalt, *Phys. Rev. Lett.* **2004**, *92*, 196403.
- [53] A. T. Hanbicki, G. Kioseoglou, M. Currie, C. S. Hellberg, K. M. McCreary, A. L. Friedman, B. T. Jonker, *Sci. Rep.* **2016**, *6*, 18885.
- [54] M. Amani, P. Taheri, R. Addou, G. H. Ahn, D. Kiriya, D. H. Lien, J. W. Ager III, R. M. Wallace, A. Javey, *Nano Lett.* **2016**, *16*, 2786.
- [55] P. K. Chow, R. B. Jacobs-Gedrim, J. Gao, T.-M. Lu, B. Yu, H. Terrones, N. Koratkar, *ACS Nano* **2015**, *9*, 1520.
- [56] C. Mai, A. Barrette, Y. Yu, Y. G. Semenov, K. W. Kim, L. Cao, K. Gundogdu, *Nano Lett.* **2014**, *14*, 202.
- [57] Y. You, X.-X. Zhang, T. C. Berkelbach, M. S. Hybertsen, D. R. Reichman, T. F. Heinz, *Nat. Phys.* **2015**, *11*, 477.
- [58] W. Yao, *Nat. Phys.* **2015**, *11*, 448.
- [59] M. S. Kim, S. J. Yun, Y. Lee, C. Seo, G. H. Han, K. K. Kim, Y. H. Lee, J. Kim, *ACS Nano* **2016**, *10*, 2399.
- [60] A. Srivastava, M. Sidler, A. V. Allain, D. S. Lembke, A. Kis, A. Imamolu, *Nat. Nanotechnol.* **2015**, *10*, 491.
- [61] M. Koperski, K. Nogajewski, A. Arora, V. Cherkez, P. Mallet, J.-Y. Veuillen, J. Marcus, P. Kossacki, M. Potemski, *Nat. Nanotechnol.* **2015**, *10*, 503.
- [62] Y.-M. He, G. Clark, J. R. Schaibley, Y. He, M.-C. Chen, Y.-J. Wei, X. Ding, Q. Zhang, W. Yao, X. Xu, *Nat. Nanotechnol.* **2015**, *10*, 497.
- [63] C. Chakraborty, L. Kinnischtzke, K. M. Goodfellow, R. Beams, A. N. Vamivakas, *Nat. Nanotechnol.* **2015**, *10*, 507.
- [64] L. C. Flatten, D. M. Coles, Z. Y. He, D. G. Lidzey, R. A. Taylor, J. H. Warner, J. M. Smith, *Nat. Commun.* **2017**, *8*, 14097.
- [65] S. F. Wu, S. Buckley, J. R. Schaibley, L. F. Feng, J. Q. Yan, D. G. Mandrus, F. Hatami, W. Yao, J. Vuckovic, A. Majumdar, X. D. Xu, *Nature* **2015**, *520*, 69.
- [66] O. Salehzadeh, M. D. Javid, N. H. Tran, I. Shih, Z. Mi, *Nano Lett.* **2015**, *15*, 5302.
- [67] R. S. Sundaram, M. Engel, A. Lombardo, R. Krupke, A. C. Ferrari, P. Avouris, M. Steiner, *Nano Lett.* **2013**, *13*, 1416.
- [68] Y. Ye, Z. L. Ye, M. Gharghi, H. Y. Zhu, M. Zhao, Y. Wang, X. B. Yin, X. Zhang, *Appl. Phys. Lett.* **2014**, *104*, 193508.
- [69] O. Lopez-Sanchez, E. A. Llado, V. Koman, A. F. I. Morral, A. Radenovic, A. Kis, *ACS Nano* **2014**, *8*, 3042.
- [70] Y. J. Zhang, T. Oka, R. Suzuki, J. T. Ye, Y. Iwasa, *Science* **2014**, *344*, 725.
- [71] W. Yang, J. Shang, J. Wang, X. Shen, B. Cao, N. Peimyoo, C. Zou, Y. Chen, Y. Wang, C. Cong, W. Huang, T. Yu, *Nano Lett.* **2016**, *16*, 1560.
- [72] L. M. Malard, T. V. Alencar, A. P. M. Barboza, K. F. Mak, A. M. de Paula, *Phys. Rev. B* **2013**, *87*, 201401(R).
- [73] N. Kumar, S. Najmaei, Q. N. Cui, F. Ceballos, P. M. Ajayan, J. Lou, H. Zhao, *Phys. Rev. B* **2013**, *87*, 161403.
- [74] H. L. Zeng, G. B. Liu, J. F. Dai, Y. J. Yan, B. R. Zhu, R. C. He, L. Xie, S. J. Xu, X. H. Chen, W. Yao, X. D. Cui, *Sci. Rep.* **2013**, *3*, 1608.
- [75] C. Janisch, Y. X. Wang, D. Ma, N. Mehta, A. L. Elias, N. Perea-Lopez, M. Terrones, V. Crespi, Z. W. Liu, *Sci. Rep.* **2014**, *4*, 5530.
- [76] H. Z. Liu, Y. L. Li, Y. S. You, S. Ghimire, T. F. Heinz, D. A. Reis, *Nat. Phys.* **2017**, *13*, 262.
- [77] R. I. Woodward, R. T. Murray, C. F. Phelan, R. E. P. d. Oliveira, T. H. Runcorn, E. J. R. Kelleher, S. Li, E. C. d. Oliveira, G. J. M. Fechine, G. Eda, C. J. S. d. Matos, *2D Mater.* **2017**, *4*, 011006.
- [78] T.-T. Carlos, P.-L. Néstor, E. A. Laura, R. G. Humberto, A. C. David, B. Ayse, L.-U. Florentino, T. Humberto, T. Mauricio, *2D Mater.* **2016**, *3*, 021005.
- [79] X. B. Yin, Z. L. Ye, D. A. Chenet, Y. Ye, K. O'Brien, J. C. Hone, X. Zhang, *Science* **2014**, *344*, 488.
- [80] Z. L. Ye, T. Cao, K. O'Brien, H. Y. Zhu, X. B. Yin, Y. Wang, S. G. Louie, X. Zhang, *Nature* **2014**, *513*, 214.
- [81] M. R. Molas, C. Faugeras, A. O. Slobodeniuk, K. Nogajewski, M. Bartos, D. M. Basko, M. Potemski, *2D Mater.* **2017**, *4*, 021003.
- [82] M. Baranowski, A. Surrente, D. K. Maude, M. Ballottin, A. A. Mitioglu, P. C. M. Christianen, Y. C. Kung, D. Dumcenco, A. Kis, P. Plochocka, *2D Mater.* **2017**, *4*, 025016.
- [83] X. X. Zhang, Y. M. You, S. Y. F. Zhao, T. F. Heinz, *Phys. Rev. Lett.* **2015**, *115*, 257403.
- [84] Y. Zhou, G. Scuri, D. S. Wild, A. A. High, A. Dibos, L. A. Jauregui, C. Shu, K. De Greve, K. Pistunova, A. Y. Joe, T. Taniguchi, K. Watanabe, P. Kim, M. D. Lukin, H. Park, *Nat. Nanotechnol.* **2017**, *12*, 856.



- [85] X.-X. Zhang, T. Cao, Z. Lu, Y.-C. Lin, F. Zhang, Y. Wang, Z. Li, J. C. Hone, J. A. Robinson, D. Smirnov, S. G. Louie, T. F. Heinz, *Nat. Nanotechnol.* **2017**, *12*, 883.
- [86] T. C. Berkelbach, M. S. Hybertsen, D. R. Reichman, *Phys. Rev. B* **2015**, *92*, 085413.
- [87] C. Mai, A. Barrette, Y. F. Yu, Y. G. Semenov, K. W. Kim, L. Y. Cao, K. Gundogdu, *Nano Lett.* **2014**, *14*, 202.
- [88] M. Danovich, V. Zolyomi, V. I. Fal'ko, *Sci. Rep.* **2017**, *7*, 45998.
- [89] M. Danovich, V. Zolyomi, V. I. Fal'ko, I. L. Aleiner, *2D Mater.* **2016**, *3*, 035011.
- [90] F. Ceballos, Q. N. Cui, M. Z. Bellus, H. Zhao, *Nanoscale* **2016**, *8*, 11681.
- [91] C. Mai, Y. G. Semenov, A. Barrette, Y. F. Yu, Z. H. Jin, L. Y. Cao, K. W. Kim, K. Gundogdu, *Phys. Rev. B* **2014**, *90*, 041414.
- [92] R. Schmidt, G. Berghauser, R. Schneider, M. Selig, P. Tonndorf, E. Malic, A. Knorr, S. M. de Vasconcelos, R. Bratschitsch, *Nano Lett.* **2016**, *16*, 2945.
- [93] G. Plechinger, P. Nagler, A. Arora, R. Schmidt, A. Chernikov, J. Lupton, R. Bratschitsch, C. Schuller, T. Korn, *Phys. Status Solidi RRL* **2017**, *11*, 1700131.
- [94] M. Amani, P. Taheri, R. Addou, G. H. Ahn, D. Kiriya, D. H. Lien, J. W. Ager, R. M. Wallace, A. Jayey, *Nano Lett.* **2016**, *16*, 2786.
- [95] Y. Hoshi, T. Kuroda, M. Okada, R. Moriya, S. Masubuchi, K. Watanabe, T. Taniguchi, R. Kitaura, T. Machida, *Phys. Rev. B* **2017**, *95*, 241403.
- [96] T. Kato, T. Kaneko, *ACS Nano* **2016**, *10*, 9687.
- [97] K. Hao, J. F. Specht, P. Nagler, L. X. Xu, K. Tran, A. Singh, C. K. Dass, C. Schuller, T. Korn, M. Richter, A. Knorr, X. Q. Li, G. Moody, *Nat. Commun.* **2017**, *8*, 1552.
- [98] W. J. Zhao, S. F. Wang, B. Liu, I. Verzhbitskiy, S. S. Li, F. Giustino, D. Kozawa, K. P. Loh, K. Matsuda, K. Okamoto, R. F. Oulton, G. Eda, *Adv. Mater.* **2016**, *28*, 2709.
- [99] D. Zheng, S. Zhang, Q. Deng, M. Kang, P. Nordlander, H. Xu, *Nano Lett.* **2017**, *17*, 3809.
- [100] M. I. Vasilevskiy, D. G. Santiago-Perez, C. Trallero-Giner, N. M. R. Peres, A. Kavokin, *Phys. Rev. B* **2015**, *92*, 245435.
- [101] O. L. Berman, R. Y. Kezerashvili, *Phys. Rev. B* **2016**, *93*, 245410.